Agricultural Water Management 266 (2022) 107583

Contents lists available at ScienceDirect

Agricultural Water Management

journal homepage: www.elsevier.com/locate/agwat

Assimilating remote sensing data into a crop model improves winter wheat yield estimation based on regional irrigation data

Ning Jin [a], Bo Tao [b], Wei Ren [b], Liang He [c,*], Dongyan Zhang [d,*], Dacheng Wang [e], Qiang Yu [f,g]

[a] Department of Resources and Environmental Engineering, Shanxi Institute of Energy, Jinzhong 030600, Shanxi, China
[b] Department of Plant and Soil Sciences, College of Agriculture, Food and Environment, University of Kentucky, KY 40506, USA
[c] National Meteorological Centre, Beijing 100081, China
[d] National Engineering Research Center for Agro-Ecological Big Data Analysis & Application, Anhui University, Hefei 230601, China
[e] State Key Laboratory of Remote Sensing Science, Aerospace Information Research Institute, Chinese Academy of Sciences, Beijing 100101, China
[f] State Key Laboratory of Soil Erosion and Dryland Farming on the Loess Plateau, Institute of Soil and Water Conservation, Northwest A&F University, Yangling 712100, Shaaxi, China
[g] School of Life Sciences, University of Technology Sydney, P.O. Box 123, Broadway, NSW 2007, Australia

ARTICLE INFO

Handling Editor: Dr. B.E. Clothier

Keywords:
Data assimilation
Remote sensing data
ChinaAgrosys crop model
Regional irrigation
Winter wheat

ABSTRACT

Irrigation plays an important role in crop yield production in arid and semi-arid regions. However, irrigation effects have not been well addressed in the application of crop models at a regional scale due to limited data availability, which constrains the reliability and accuracy of simulation results. Assimilating remote sensing information into crop models can provide a viable approach to reduce associated uncertainties. In this study, regional irrigation data for winter wheat (*Triticum aestivum* L.) grown on the Loess Plateau was used to calibrate and validate the ChinaAgrosys (China Agricultural System) crop model at site and regional scales. Remote sensing data was then assimilated into the ChinaAgrosys crop model under four assimilation schemes. Two remotely sensed assimilation state variables (i.e., LAI and NDVI) and two assimilation algorithms (i.e., PSO (Partical swarm optimization) and SCE-UA (Shuffled complex evolution)) were considered. During the winter wheat growing season on the Loess Plateau, 30.6% of the wheat production area was irrigated once, 6.7% was irrigated two times, 3.7% was irrigated three times, and the remaining wheat area was rainfed. The R^2 values between maturity date, LAI, and yield simulated by the ChinaAgrosys crop model and observations at 21 agrometeorological stations on the Loess Plateau were greater than 0.73, 0.44, and 0.60, respectively, during 2010–2015. The accuracy and spatial heterogeneity of winter wheat yield estimation were effectively improved by assimilating remote sensing data into the ChinaAgrosys crop model based on regional irrigation data. Under the four assimilation schemes, the combination of PSO+NDVI produced the highest accuracy for yield estimation in Hongtong county (92.8%), followed by SCE-UA+NDVI (92.0%). Our results demonstrated the importance of accounting for the spatial heterogeneity of water availability when applying a crop model in arid and semi-arid regions. Additionally, our analysis regarding different assimilation state variables and algorithms indicated that both simulation accuracy and calculation efficiency should be considered when assimilating remote sensing data into a crop model for simulating crop growth at regional scales.

1. Introduction

Crop models can simulate photosynthesis, respiration, transpiration, and dry matter distribution during periods of crop growth and yield production. Over recent decades, crop models have been widely used to investigate climate change impacts on crop yield (Bocchiola et al., 2013), to schedule farmland irrigation (Chimonyo et al., 2016), and to analyze effects of drought stress on growth crop and yield (Yin et al., 2014). However, most crop models were originally developed for plot/field-scale studies and their regional application has been constrained by the availability of input parameters regarding meteorology, soil characteristics, agricultural management, etc. (Lv et al., 2016). Satellite remote sensing has rapidly developed and plays an important role in quantifying crop planted area, growth monitoring, yield

* Corresponding authors.
E-mail addresses: heliang@cma.gov.cn (L. He), zhangdy@ahu.edu.cn (D. Zhang).

https://doi.org/10.1016/j.agwat.2022.107583
Received 12 August 2021; Received in revised form 28 February 2022; Accepted 1 March 2022

forecasting, and drought assessment at regional scales (Sakamoto et al., 2013; Park et al., 2016; Chen et al., 2018). Combining satellite remote sensing data with crop models can result in continuous spatiotemporal modeling of crop growth processes (Jin et al., 2018b; Huang et al., 2019), and can provide strong support for dynamic monitoring of crop growth and yield production at regional scales. Data assimilation methods that combine the advantages of crop modeling and remote sensing data have been widely developed in recent years (Ines et al., 2013; Hu et al., 2019). This process is implemented by continuously integrating a variety of observation data, and constantly adjusting the trajectory of simulations within the dynamic framework of the crop model (Huang et al., 2015a). The variables assimilated into a crop model may include leaf area index (LAI), normalized difference vegetation index (NDVI), evapotranspiration (ET), soil moisture, enhanced vegetation index (EVI), etc. (de Wit and van Diepen, 2007; Curnel et al., 2011; Ma et al., 2013; Huang et al., 2015b; Guo et al., 2019). Previous studies have shown that crop model simulation results were improved by assimilating biophysical variables obtained from remote sensing data (Kang and Özdoğan, 2019; Lei et al., 2020). In contrast, the process of upscaling irrigation data to regional scale requires further study. Irrigation activities are influenced by many factors, including water availability, irrigation water price, crop growth conditions, farmers' willingness to irrigate a crop, etc. The timing and amount of irrigation events on farmland have a great amount of uncertainty, thereby increasing the difficulties in obtaining irrigation data at a regional scale. Currently, studies regarding regional irrigation data are mainly focused on classifying crop areas as either irrigated or rainfed (Pervez et al., 2014; Deines et al., 2019; Xie et al., 2019). However, realistically estimating regional crop growth requires information regarding irrigation timing and amount, which currently cannot be derived from existing irrigation data sets.

Agricultural production on the Loess Plateau in China is largely constrained by water availability. Irrigation plays a critical role in ensuring crop productivity. In dry years, irrigated wheat yield can be 2.3 times greater than rainfed wheat yield (Jin et al., 2016b). The ability of a crop model to accurately simulate yield production and water consumption in this region is compromised by the lack of accurate regional irrigation data. Usually, a crop in an entire study area is assumed to be rainfed or is assumed to use a standard irrigation scenario (Zhang et al., 2013; Wang et al., 2015; Adhikari et al., 2016). Different water availability for crops has been considered in some studies, but the spatial resolution has been coarse, and the irrigated and rainfed conditions were the same for different crops (Mo et al., 2005). In general, it is difficult to get reliable irrigation data at a regional scale, and therefore the spatial heterogeneity in irrigation data is given less attention when applying a crop model at a regional scale. Furthermore, the influence of spatial heterogeneity of irrigation data on simulation results is seldom considered for the subsequent assimilation of remote sensing data into a crop model (De et al., 2012; Huang et al., 2015b; Jin et al., 2016a; Gilardelli et al., 2019). Ignoring the spatial heterogeneity of irrigation data may lead to some uncertainties for the simulation results of crop models in arid and semi-arid regions.

In this study, wheat production areas on the Loess Plateau were classified as either irrigated and rainfed. Irrigation times were then assumed based on the local irrigation practices and the estimated wheat yield from a light use efficiency model. Taking into account the spatial heterogeneity of irrigation data on the Loess Plateau can improve the accuracy and reliability of yield estimation when assimilating remote sensing data into the ChinaAgrosys (China Agricultural System) crop model. The major scientific objectives of this study were to: (1) extract regional irrigation data for winter wheat production on the Loess Plateau; (2) estimate winter wheat LAI at 250-m spatial resolution using the PROSAIL radiation transfer model; (3) evaluate the performance of ChinaAgrosys on the Loess Plateau; (4) couple ChinaAgrosys with the PROSAIL radiation transfer model, and build schemes for assimilating remote sensing data based on spatial irrigation data into ChinaAgrosys.

2. Materials and methods

2.1. Study area

The Loess Plateau is located between 32–41°N and 103–114°E with an area of 648,700 km^2, including 341 counties in Shanxi, Shaanxi, Ningxia, Henan, Gansu, Inner Mongolia, and Qinghai provinces/autonomous regions. The southeast Loess Plateau is lower than the northwest, and the elevation varies from 500 m to about 3000 m. The Loess Plateau is under the influence of a continental monsoon climate, and is a transition zone changing from semi-humid to semi-arid climate. Precipitation increases from the northwest (150–250 mm) to the southeast (above 600 mm), and shows large inter-annual variation. Precipitation in wet years can be 2–5 times greater than precipitation in dry years.

In this study, we selected 158 counties that planted winter wheat in the central and southern Loess Plateau, which accounted for 46.3% of the total counties (Fig. 1). The average winter wheat yields in Gansu, Ningxia, Shaanxi, Shanxi, and Henan provinces were 2426, 2206, 4022, 3031, and 4382 kg ha^{-1} in 2011, respectively. Winter wheat is usually planted in October and harvested in June of the following year. Precipitation during the winter wheat growing season is far less than the amount needed to meet the demand for crop growth and yield production. Irrigation plays an important role in producing high and stable winter wheat yield.

2.2. Data

2.2.1. Remote sensing data

The remote sensing data used in this study included MOD13Q1 NDVI data (16-day, 250-m resolution) and MOD15A2 LAI data (8-day, 1000–m resolution) during the years 2010–2015. Two scenes were needed for the MODIS data to cover the entire Loess Plateau (path/row: h26v05 and h27v05). After applying re-projection, mosaic, and merging processing to the MODIS data, 1884 × 3815 pixels in the study area were obtained using the vector shapefile of the Loess Plateau boundary.

2.2.2. Meteorological, soil, and ground observation data

Meteorological data for the 158 counties on the Loess Plateau were obtained for the period of 2010–2015, including daily mean temperature, maximum temperature, minimum temperature, sunshine hours, precipitation, and wind speed. A multivariate linear regression model that considered geographic effects (longitude, latitude, elevation, slope, and aspect) was used to interpolate meteorological data elements at a spatial resolution of 250 m to match the remote sensing data (Jin et al., 2018a). The spatially explicit soil properties obtained from Dai et al. (2013) included soil texture, saturated water content, wilting coefficient, and field water holding capacity.

The ground observation data for winter wheat during 2012–2014 were collected from the Water-saving Agricultural Experiment Station of Northwest A&F University at Yangling (Fig. 1). The winter wheat cultivar was Xiaoyan22. The data for the period of 2012–2013 and 2013–2014 were used to calibrate and validate, respectively, the ChinaAgrosys crop model. There were a total of 21 winter wheat agrometeorological stations across the Loess Plateau. The observation data included planting date, maturity date, LAI, yield, etc., which were used to evaluate the applicability of ChinaAgrosys. The LAI data at jointing and heading stages for six agrometeorological stations in Shanxi province were used to validate LAI values that the look-up table (described later) generated and that ChinaAgrosys simulated.

2.3. ChinaAgrosys crop model and parameter sensitivity analysis

ChinaAgrosys is a comprehensive soil-vegetation-atmosphere model in which photosynthesis, transpiration, and stomatal conductance models were extended from leaf to canopy scale by integrating the leaf

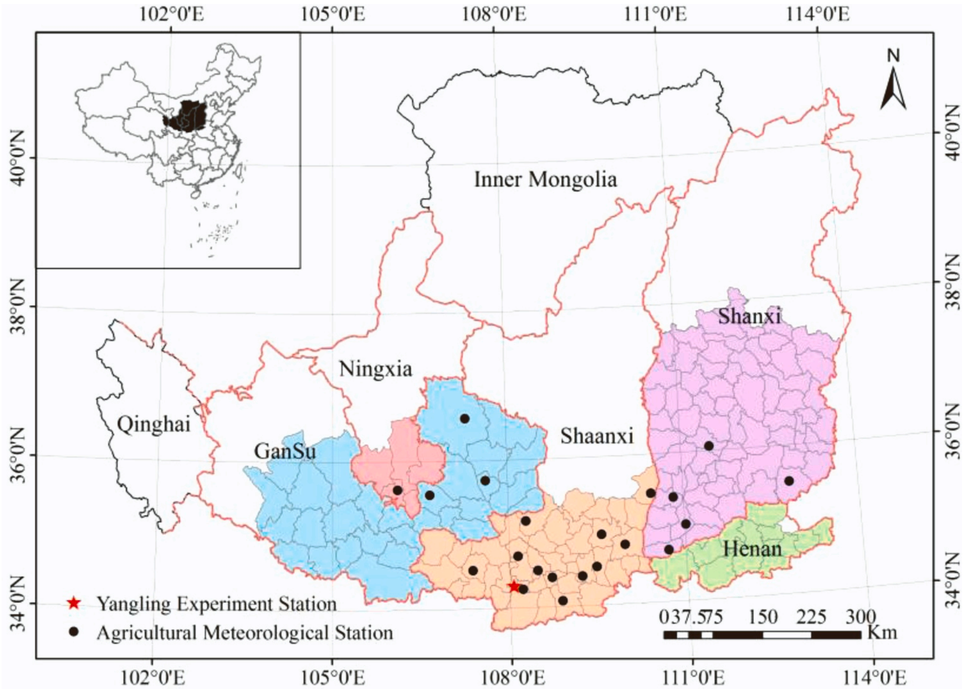

Fig. 1. The Loess Plateau study area, counties with winter wheat (colored areas), Yangling experimental station, and 21 winter wheat agrometeorological stations.

water potential dynamic model with the hydrothermal transfer and photosynthetic models in SPAC (Soil-Plant-Atmosphere Continuum). ChinaAgrosys considers the crop growth and hydrothermal transfer process, and consists of three sub-modules, i.e., soil, crop growth, and micro-meteorology. Details regarding ChinaAgrosys can be found in Wang et al. (2007).

The major parameters in ChinaAgrosys affecting physiological processes controlling crop growth and development include the developmental rate parameters (c0, c1, nondimensional quantity), LAI parameters (a0, a1, a2, a3, nondimensional quantity), crop specific parameters (alpha0, initial quantum efficiency; v0, max photosynthesis rate, μmol m^{-2} s^{-1}), and yield parameters (b0, b1, b2, nondimensional quantity). The most sensitive parameters with respect to crop development and yield production were selected based on an analysis of the influence of the interrelationships between parameters from simulation results. This process was helpful in selecting the optimal values of parameters for assimilating remote sensing data into ChinaAgrosys, thereby improving the efficiency of the optimizing algorithm and reducing the computational requirements. The global sensitivity analysis of the 11 parameters in ChinaAgrosys was implemented using the EFAST (Extended Fourier amplitude sensitivity test) method based on the observed LAI and yield data at the Yangling experimental station from 2012 to 2013.

The framework of the sensitivity calculation was constructed using the sensitivity package written in the R program (http://www.r-project.org/), and the executable file and parameters file in ChinaAgrosys were called to calculate the sensitivity for the 11 parameters. In the EFAST method, the number of calculations for a single process was $n \times p$, where n is the number of samples and p is the number of parameters.

2.4. Classification of irrigated and rainfed wheat, yield estimation, and irrigation criteria

The winter wheat planted area on the Loess Plateau was extracted based on the variation of the NDVI time series (Jin et al., 2016b). Yield was estimated using a light use efficiency model (Jin et al., 2018a). The timing and amount of irrigation for winter wheat was estimated based on the classification results and the estimated winter wheat yield, given that crop growth and yield production in the study areas are largely determined by water availability. Specifically, the irrigation amount was set as 0 mm for rainfed wheat; three irrigation levels were used for irrigated wheat: irrigated once (when yield<4500 kg/ha; 1 April 2011), irrigated twice (when 6000 kg/ha>yield>4500 kg/ha; 1 December 2010 and 1 April 2011), and irrigated three times (when yield>6000 kg/ha; 1 December 2010, 1 April 2011, and 15 May 2011). The irrigation amount was 50 mm for each irrigation event according to the typical agricultural production practices on the Loess Plateau.

2.5. PROSAIL radiation transfer model and LAI inversion

2.5.1. PROSAIL radiation transfer model

The PROSAIL radiation transfer model consists of two sub-modules (i.e., the PROSPECT model and the SAIL model). The PROSPECT model simulates hemisphere directional reflectance and transmittance at leaf scale in the wavelength range 400–2500 nm. Then leaf reflectance and transmittance are used to drive the SAIL model to simulate canopy reflectance. The PROSAIL 5B radiation transfer model used in this study was downloaded from http://teledetection.ipgp.jussieu.fr/prosail. Details of the PROSAIL 5B model can be found in Jacquemoud et al. (2009).

2.5.2. LAI inversion

Leaf area index is an important input variable used in many land surface models, and has been widely used in crop growth monitoring and yield predication (Sakamoto et al., 2013). When assimilating remote sensing data into a crop model at a regional scale, results are mainly influenced by the accuracy of retrieved LAI. Generally, there are two major ways to retrieve LAI using satellite remote sensing data, i.e., empirical/semi-empirical model inversion and physical model inversion (Pasolli et al., 2015). At present, the main data sources used to retrieve the LAI product at large scales are MODIS, GLASS, and other satellite remote sensing data at medium spatial resolutions. The temporal and spatial resolution of these LAI products are 8 days to 1 month and 1–10 km, respectively. The MODIS LAI product is not crop specific, and the LAI values of farmland are lower than ground observations (Duveiller et al., 2013). Moreover, image resolution is too coarse to be used on the Loess Plateau due to the highly fragmented farmland in this region. Therefore, it is difficult to directly assimilate the 1-km MODIS LAI product into a crop model, which may reduce the spatial heterogeneity in the simulation results. In this study, LAI at 250-m spatial resolution was retrieved for the Loess Plateau based on an NDVI-LAI look-up table derived from the PROSAIL radiation transfer model (Fig. 2).

2.5.3. Hyperspectral reflectance data of winter wheat

Hyperspectral reflectance data for the winter wheat canopy were measured with the Analytical Spectral Devices (ASD) Field Spec Pro FR (350–2500 nm) spectroradiometer. Instrument calibration was performed using a standard reference board before and after each measurement of the reflectance spectrum. Measurements were made between 10:00 and 15:00 when the sky was cloudless and wind speed was low. The angle of the spectroradiometer was set as 25° with a height of 1.3 m. Each winter wheat sample area was measured 10 times. The spectroradiometer data were then used to validate the simulation results of the PROSAIL radiation transfer model.

2.5.4. Conversion between hyperspectral reflectance data and multispectral reflectance data

The observed and simulated winter wheat canopy reflectance ranges were 350–2500 nm and 400–2500 nm, respectively. The MODIS image was comprised of multispectral reflectance data. The MODIS image data were associated with the hyperspectral data using the spectral response function. The wide-band reflectance was estimated as follows (Steven et al., 2003):

$$\rho = \frac{\int I(\lambda)R(\lambda)\varphi(\lambda)d\lambda}{\int I(\lambda)\varphi(\lambda)d\lambda} \tag{1}$$

where ρ is the reflectance of the corresponding band of the satellite sensor; I is the ground-measured incident solar radiation; R is the vegetation canopy reflectance; λ is the wavelength; φ is the spectral response function of the corresponding satellite sensor band, including blue, green, red, near infrared, shortwave infrared bands, etc. The spectral response function in the spectral library was linearly interpolated to match the spectral resolution of the observed and simulated canopy reflectance.

2.5.5. LAI estimation using the look-up table inversion method

One MODIS pixel at 1-km spatial resolution would contain 16 pixels at 250-m spatial resolution. If the original MODIS LAI data were directly used, then all 16 pixels would have the same value. Doing so would greatly reduce the spatial heterogeneity in the resulting data simulated by the crop model. Therefore, it was necessary to invert winter wheat LAI at 250-m spatial resolution before assimilating remote sensing data into the crop model on the Loess Plateau.

The look-up table is a relatively simple method to invert LAI based on the radiation transfer model. The method can produce a global optimum solution and avoid the shortcoming of the neural network that easily obtains the local optimal solution. Additionally, the computation complexity and abnormality are lower than seen for numerical optimization methods. During the LAI inversion, a look-up table containing the LAI values generated by the PROSAIL radiation transfer model and the corresponding NDVI estimated using canopy reflectance was established based on the forward radiation transfer model.

2.6. PSO and SCE-UA optimization algorithms and objective functions

Particle Swarm Optimization (PSO) is an intelligent algorithm used to simulate bird clustering and foraging that was developed at the end of the twentieth century (Kennedy and Eberhart, 1995). Details regarding the PSO algorithm can be found in Li et al. (2015). The global optimization algorithm of SCE-UA (Shuffle Complex Evolution method) has been widely used in parameter calibration for hydrological watershed models (Duan et al., 1994).

The continuous data assimilation algorithms of PSO and SCE-UA were used in this study. By continuously adjusting the parameters of the model, the objective function reached the minimum value when the model simulations (of LAI or NDVI) agreed best with the observations. The objective function F_{min} was calculated as:

$$F_{\min} = \sqrt{\frac{\sum_{i=1}^{n}\left(\frac{X_{\text{model},i}-X_{\text{obs},i}}{X_{\text{obs},i}}\right)^2}{n}} \tag{2}$$

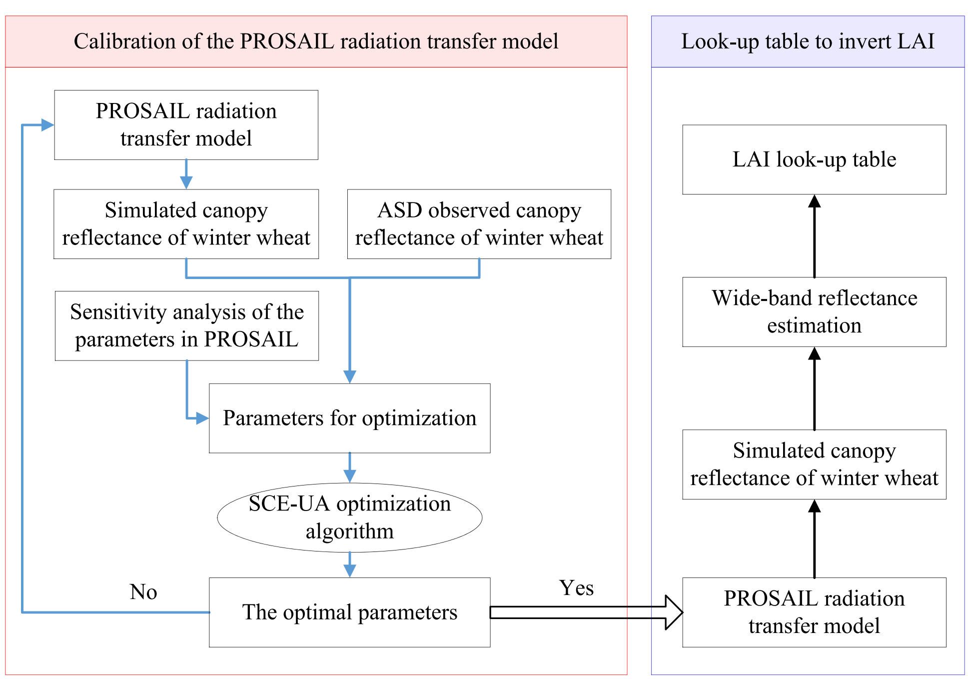

Fig. 2. Flowchart of the LAI inversion method using the PROSAIL radiation transfer model.

where a smaller value of F_{min} means a more accurate simulation result for the model. In the equation, $i = 1, 2, 3, \ldots, n$, n is the number of observations, and $X_{\mathrm{model,i}}$ and $X_{\mathrm{obs,i}}$ are the i^{th} model simulation result and observation, respectively.

2.7. Assimilation of remote sensing data into the ChinaAgrosys crop model

The assimilation of remote sensing data into ChinaAgrosys included the three major parts of (1) crop model, (2) observation data, and (3) assimilation algorithm. The crop model supplied the dynamic framework and simulated the crop growth processes by constantly updating the state variables. The observation data included remote sensing data and ground observation data, etc. Determining the best match between the model simulation values and observation data was realized using the data assimilation algorithm. There are two ways to couple the crop model with remote sensing data at spatiotemporal scale (Table 1):

(1) LAI as the assimilation state variable (Fig. 3). The difference between LAI values that ChinaAgrorys simulates and the inverted remote sensing data is reduced by continuously adjusting the parameters of the crop model using the optimization algorithm. The optimal parameters are obtained when the objective function reaches its minimum value, and then crop yield is estimated based on these parameters.

(2) NDVI as the assimilation state variable (Fig. 3). ChinaAgrosys and the PROSAIL radiation transfer model are coupled (the LAI estimated by ChinaAgrosys is input to the PROSAIL radiation transfer model), and NDVI is calculated based on the simulated canopy reflectance. The difference between NDVI that the coupled model generates and that remote sensing data estimates is reduced by continuously adjusting the parameters of the crop model using the optimization algorithm. The optimal parameters are obtained when the objective function reaches its minimum value, and then crop yield is estimated based on these parameters.

The assimilation framework used four modules: (1) the main module, whose function was to call the crop model/radiation transfer model and submodule for the objective function; (2) the settings for the crop model parameters, reading the simulation result, and calling the radiation transfer model module; (3) the radiation transfer model module; and (4) the objective function module. When running the coupled data assimilation scheme, data for latitude, longitude, altitude, planting date, irrigation data, soil property parameters, inverted LAI, and meteorological parameters for wheat pixels were written into the corresponding '.site' and '.control' files. Then the crop model and radiation transfer model were continuously called using the optimization algorithm. During this process, the simulated LAI or NDVI was compared with the corresponding state variable to obtain the optimal combination of parameters (Fig. 4).

Table 1
Schemes for assimilating remote sensing data into the ChinaAgrosys crop model.

Assimilation algorithm	No.	Assimilation state variable	Assimilation scheme
PSO	1	LAI	ChinaAgrosys-LAI-MODIS
	2	NDVI	ChinaAgrosys-LAI-PROSAIL-NDVI-MODIS
SCE-UA	3	LAI	ChinaAgrosys-LAI-MODIS
	4	NDVI	ChinaAgrosys-LAI-PROSAIL-NDVI-MODIS

3. Results

3.1. Spatial distribution of irrigation times for winter wheat on the Loess Plateau

Irrigated and rainfed wheat areas on the Loess Plateau were classified according to water availability. Rainfed wheat accounted for 60% of the winter wheat area planted on the Loess Plateau, and the rest was irrigated wheat. Irrigation times were different throughout the irrigated wheat area (Fig. 5). The proportion of the wheat area irrigated one, two, and three times on the Loess Plateau was 30.6%, 6.7%, and 2.7%, respectively. Hence, water availability for winter wheat on the Loess Plateau exhibited great spatial heterogeneity. The difference in water availability for winter wheat on the Loess Plateau should be taken into account when applying a crop model at a regional scale in order to reduce the uncertainty in simulation results that may be induced by the uncertain regional irrigation data.

3.2. Applicability assessment of the ChinaAgrosys crop model on the Loess Plateau

3.2.1. Parameter sensitivity analysis for ChinaAgrosys

The results of the global sensitivity analysis of parameters for ChinaAgrosys showed that the five LAI parameters with the greatest first-order sensitivity index values were c1, b2, c0, b0, and b1 with sensitivity values of 30.4%, 23.9%, 21.7%, 11.6%, and 10.5%, respectively. The five LAI parameters with the greatest global sensitivity index values were c1, b2, c0, b1, and b0 with sensitivity values of 39.1%, 35.2%, 25.7%, 23.7%, and 22.7%, respectively. The five yield parameters with the greatest first-order sensitivity index values were b2, c1, c0, a0, and b0 with sensitivity values of 19.6%, 13.7%, 13.3%, 10.2%, and 9.7% respectively. And the five yield parameters with the greatest global sensitivity index values were b2, a0, c1, c0, and a2 with sensitivity values of 31.9%, 23.7%, 23.5%, 22.9%, and 22.6%, respectively (Fig. 6). Based on the above results, the parameters of c0, c1, and b2 were selected for optimization during the following assimilation of remote sensing data into ChinaAgrosys. The initial, minimum, and maximum values of the optimized parameters are shown in Table 2.

Parameter variation in ChinaAgrosys induced corresponding changes in maturity date, LAI, biomass, and yield for winter wheat. LAI was used as an example to demonstrate the influence of the variation of c0, c1, and b2 (Fig. 7). The variation of LAI with changing c0 and c1 were generally similar, as LAI increased with the increasing c0 and c1 before the heading stage and vice versa after the heading stage. Moreover, the maximum LAI value and the period of occurrence were also influenced by c0 and c1. The b2 parameter mainly affected the maximum value of LAI before and after the heading period. LAI tended to decrease as b2 increased.

3.2.2. ChinaAgrosys crop model evaluation at site and regional scales on the Loess Plateau

The ChinaAgrosys crop model was calibrated using the observations at the Yangling experimental station for the period 2012–2013. Simulated LAI and cumulative biomass were slightly lower at the early and late winter wheat growth stages. Overall, the variations of simulated LAI over time were consistent with observations (Fig. 8).

Simulations with the ChinaAgrosys crop model were evaluated against observations at 21 winter wheat agrometeorological stations across the Loess Plateau for the period 2010–2015. These regional observations included maturity date, LAI at jointing and heading stages, and yield production. ChinaAgrosys simulated values comparable with observations for the study region. The R^2 values between simulated and observed maturity dates were greater than 0.73, and R^2 values for LAI and yield were greater than 0.44 and 0.60, respectively (Fig. 9).

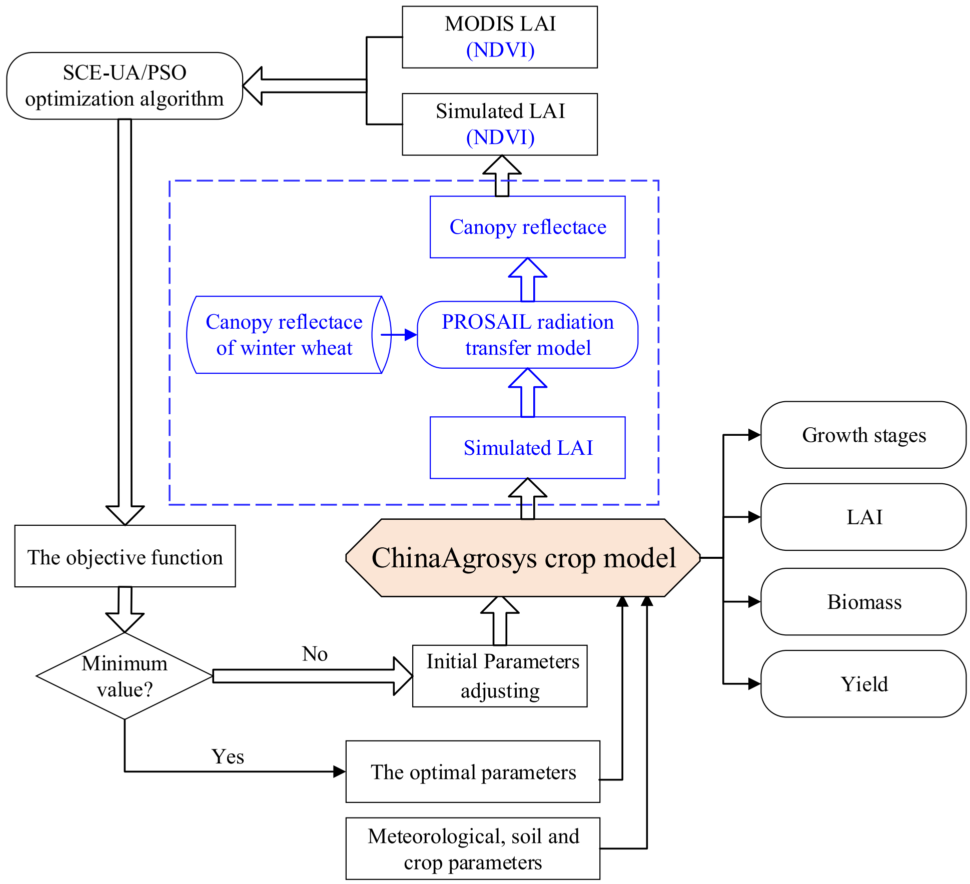

Fig. 3. Framework for assimilating remote sensing data into the ChinaAgrosys crop model. The blue section indicates the coupling of the PROSAIL radiation transfer model with the NDVI state variable. Without the blue section, the assimilation state variable is leaf area index (LAI).

3.3. Inversion of LAI at 250-m spatial resolution for winter wheat on the Loess Plateau

3.3.1. Calibration and validation of the PROSAIL radiation transfer model

Parameter ranges for the PROSAIL radiation transfer model were determined on the basis of a priori knowledge of field measurements and relevant literature (Pasolli et al., 2015; Casas et al., 2014). The parameter settings were determined based on the sensitivity analysis (Table 3).

The parameter sensitivities of the model-simulated results were evaluated by continuously changing one of the parameters in the PROSAIL radiation transfer model. Our results (Fig. 10) showed that: (1) the sensitive band for the chlorophyll parameter Cab was 550 nm, and reflectance increased with increasing Cab; (2) reflectance increased with increasing hot spot coefficient (hspot), most noticeably in the near-infrared band; (3) reflectance decreased with increasing average leaf inclination (LIDFa), most noticeably in the near-infrared band; (4) reflectance increased with increasing view zenith angle (tto), most noticeably in the near-infrared band; (5) reflectance decreased with increasing solar zenith angle (tts), most noticeably in the near-infrared band.

Based on the ASD-observed canopy reflectance of winter wheat, the sensitive parameters for the PROSAIL radiation transfer model were optimized using the SCE-UA algorithm. Simulated canopy reflectance agreed well with observations (Fig. 11). Differences between the simulated results and observations were larger in the near-infrared band than in the visible band. Overall, the optimized PROSAIL radiation transfer model provided useful data to establish the LAI look-up table.

3.3.2. Validation of inverted LAI on the Loess Plateau

Inverted LAI from the look-up table and MODIS LAI were evaluated using the ground-observed LAI at winter wheat jointing and heading stages at six winter wheat agrometeorological stations in Shanxi province from 2010 to 2015. The R^2 between look-up table LAI and ground-observed LAI was greater than 0.54, indicating a good relationship (Fig. 12). The MODIS pixels at 1-km spatial resolution were heavily influenced by the effect of mixed pixels, and resulted in lower LAI values for MODIS than for the look-up table inverted LAI and ground-observed LAI.

3.4. Assimilation of remote sensing data into the ChinaAgrosys crop model

3.4.1. Site level data-model assimilation

Winter wheat growth and development during the 2013–2014 growing season were evaluated using the four schemes to assimilate remote sensing data into ChinaAgrosys. The greatest maximum LAI value (Fig. 13) was seen for LAI obtained with NDVI as the assimilation state variable, followed by the look-up table LAI as the assimilation state variable, the ChinaAgrosys crop model simulation without assimilation, and MODIS LAI as the assimilation state variable (lowest maximum LAI). The corresponding R^2 values between the simulated LAI under the four assimilation schemes and observed LAI were 0.73, 0.79, 0.75, and 0.86, and the RMSE values were 0.89, 0.53, 0.59, and 2.52, respectively. The LAI generated by assimilating MODIS LAI into the ChinaAgrosys crop model was very low because it was influenced by the low values of MODIS LAI during the entire winter wheat growing season. The MODIS LAI of winter wheat at the Yangling station was somewhat larger in 2013–2014 compared with MODIS LAI shown in Fig. 12. This is likely due to the highly fragmented planted areas of winter wheat at the agrometeorological stations, where MODIS pixels suffered more effects

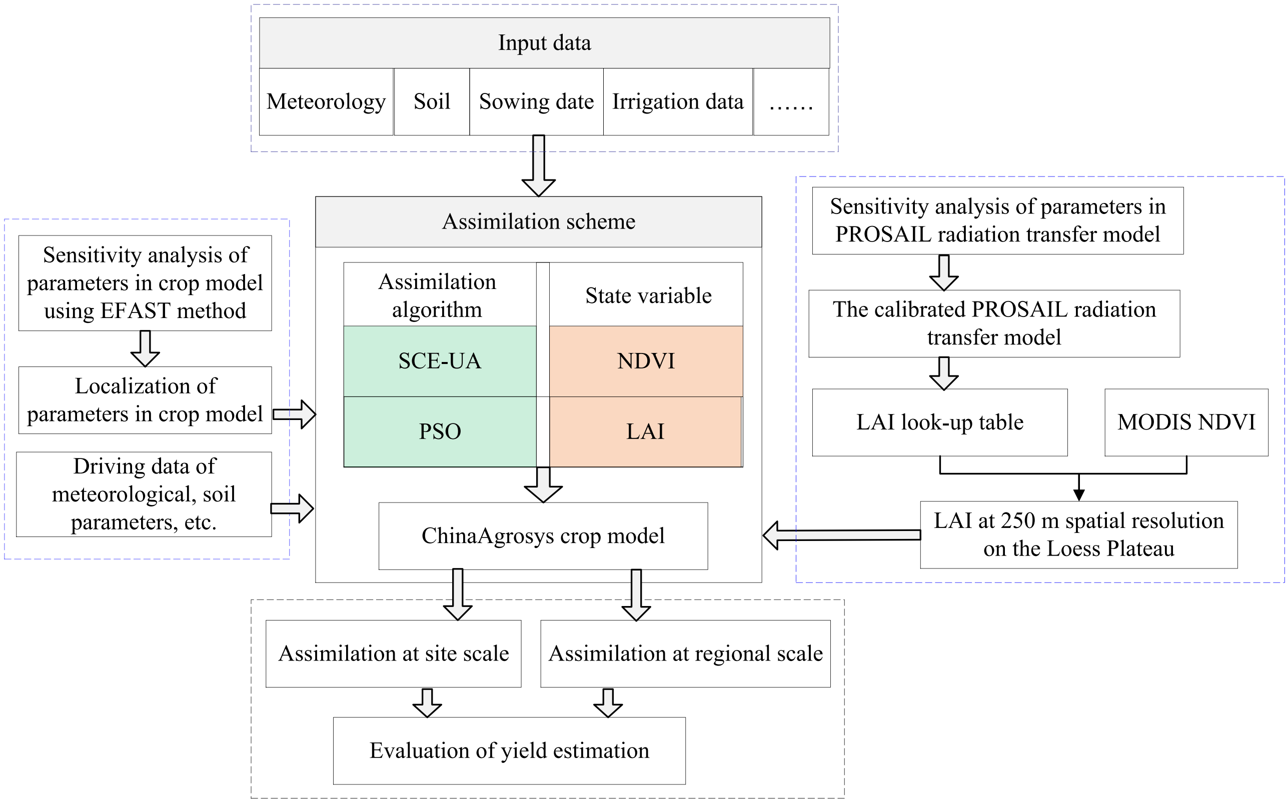

Fig. 4. Flowchart for estimating winter wheat yield based on the assimilation of remote sensing data into the ChinaAgrosys crop model.

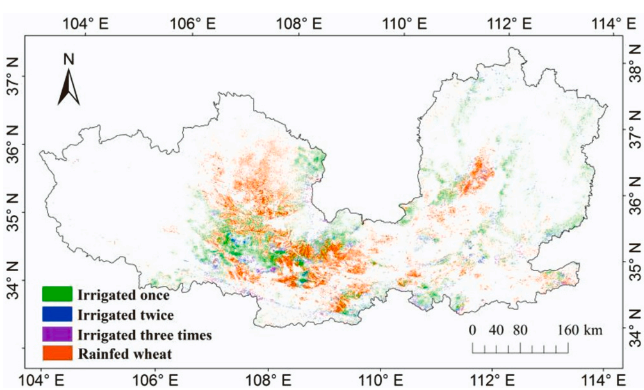

Fig. 5. Spatial distribution of number of irrigation events during the winter wheat growing season on the Loess Plateau, China.

of mixed pixels. The simulation results were improved somewhat by assimilating external remote sensing data into the crop model. Compared with the simulation results from ChinaAgrosys without assimilation, the R^2 between the simulated and observed LAI values was improved by assimilating NDVI or look-up table LAI into the crop model, and the changes in simulated LAI over time agreed well with the growth and development of winter wheat. The RMSE between observed LAI and simulated LAI generated by assimilating NDVI into ChinaAgrosys was the smallest.

The accuracy of the simulated yield under the four assimilation schemes was 93.6%, 92.1%, 91.9%, and 91.8% for the combinations of PSO+NDVI, SCE-UA+NDVI, SCE-UA+LAI, and PSO+LAI, respectively (Table 4). Accuracy was highest for the PSO+NDVI scheme, and there were little differences between the other three schemes. The order of the assimilation efficiency (based on computation time) from high to low efficiency was PSO+LAI, PSO+NDVI, SCE-UA+NDVI, and SCE-UA+LAI, respectively. Overall, the assimilation using the SCE-UA algorithm took more time than the PSO algorithm. During the data assimilation process, continuous data assimilation algorithms such as PSO and SCE-UA are very dependent on the accuracy of the external observation data due to the constraints of the algorithms.

3.4.2. *Regional scale data model assimilation*

It was difficult to implement the assimilation of remote sensing data into ChinaAgrosys for all of the 3822,830 wheat pixels on the Loess Plateau because of the low assimilation efficiency observed at the site scale for the Yangling station. Therefore, Hongtong county was selected as a representative study area for the assimilation of remote sensing data into ChinaAgrosys. There were 206 × 199 pixels contained in Hongtong county, of which 4881 pixels were winter wheat, and it took about 2.4–5.9 days to implement the assimilation of remote sensing data into ChinaAgrosys. Based on the estimated planting date and irrigation data for winter wheat, the assimilation of remote sensing data into ChinaAgrosys was implemented using two state variables (NDVI and LAI) and two assimilation algorithms (PSO and SCE-UA). The accuracy of the yield estimation under the four assimilation schemes is shown in Table 5. The yield simulation accuracy of the four assimilation schemes in Hongtong county in 2011 (ordered high to low) was PSO+NDVI (92.8%), SCE-UA+NDVI (92.0%), PSO+LAI (91.0%), and SCE-UA+LAI (89.1%). Overall, the accuracy was higher when NDVI was used as assimilation state variable than when LAI was used.

The spatial heterogeneity of rainfed wheat yield was significantly larger than that of irrigated wheat yield in Hongtong county (the average values of Moran's I (Moran, 1950) for rainfed and irrigated wheat were 0.40 and 0.17, respectively) (Fig. 14 and Fig. 15). Rainfed wheat yield is largely determined by precipitation conditions, resulting in widely varying yield with large spatial fluctuations. The area of Hongtong county is 1563 km^2, and irrigation practices are roughly similar throughout the region. Irrigated wheat yield is relatively stable and exhibits less spatial fluctuation. The estimated yield was higher for

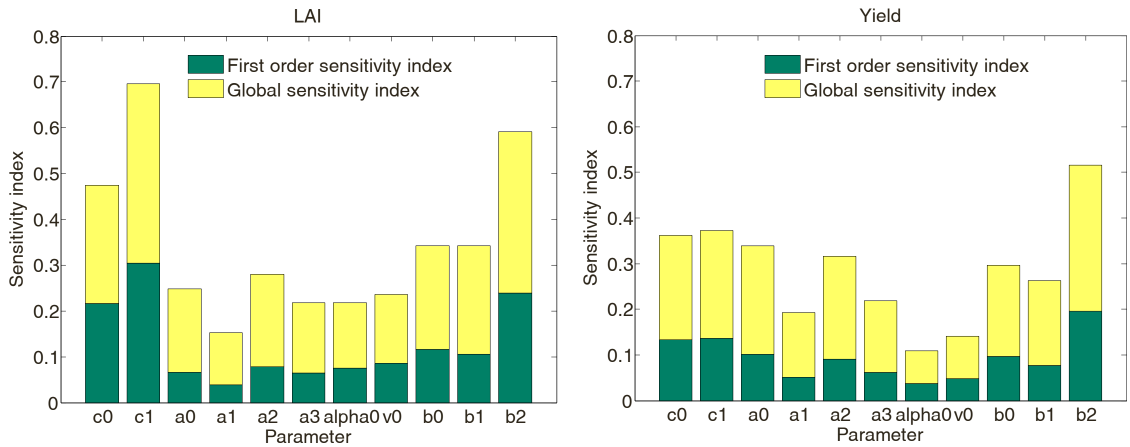

Fig. 6. Sensitivity analysis of parameters in the ChinaAgrosys crop model using the EFAST method.

Table 2
Initial, minimum, and maximum values of parameters selected for optimization in the ChinaAgrosys crop model.

Parameters	Initial value	Minimum value	Maximum value
c0	1.00E-04	6.00E-05	9.00E-04
c1	8.50E-07	6.50E-07	1.05E-06
b2	5.65	5.10	7.30

irrigated wheat than for rainfed wheat using ChinaAgrosys without the assimilation of remote sensing data. The simulation results were significantly improved by taking into account the regional irrigation data for winter wheat. The spatial patterns and values of the simulated rainfed wheat yields were similar to the yields obtained using a light use efficiency model. The simulated irrigated wheat yields using a light use efficiency model were higher at some pixels, and the results exhibited less spatial heterogeneity than those obtained with the assimilation schemes (Moran's I for the light use efficiency model was relatively larger). Compared with the results of ChinaAgrosys without assimilation of remote sensing data, the accuracy and spatial heterogeneity of the estimated yield were further improved not only by assimilating remote sensing data into ChinaAgrosys, but also by taking into account the regional irrigation data for winter wheat (for irrigated wheat, the average Moran's I under the four assimilation schemes was 0.22, which was smaller than the value of 0.45 that was the result of ChinaAgrosys without assimilation of remote sensing data).

4. Discussion

4.1. Spatial heterogeneity of irrigation data used for crop modeling

Irrigation plays an important role in crop growth, development, and yield production in arid and semi-arid regions, but the spatial heterogeneity of irrigation data has been infrequently considered when applying crop models at regional scales (Kang et al., 2019; Hu et al., 2019). Most of the time, crops in study areas have been assumed to be rainfed or set to uniform irrigation scenarios (de Wit and van Diepen, 2007; Curnel et al., 2011; Huang et al., 2015a). The differences between irrigated and rainfed crops have been recognized in some studies, but the spatial heterogeneity of irrigation data for different crops and irrigation times must be further studied (Mo et al., 2005; Gilardelli et al., 2019). On the one hand, the application of crop models at regional scales faces the problem of upscaling irrigation data, but it is difficult to obtain regional irrigation data because irrigation activities are affected by many factors (Xie et al., 2019). On the other hand, the spatial heterogeneity of irrigation data at regional scales is seldom considered when assimilating remote sensing data into crop models. Consequently, the reliability of the crop modeling results may be reduced due to uncertainty in the regional irrigation data. Moreover, the uncertainty may be further transferred to the results of the crop model with assimilated remote sensing data.

Some studies have focused on classifying irrigated and rainfed crops, and the major methods used have been digital, unsupervised, and supervised classification (Pervez et al., 2014). The Food and Agriculture Organization (FAO), United States Geological Survey (USGS), and International Water Management Institute (IWMI) have published global irrigation maps (Loveland et al., 2000; Ozdogan and Gutman, 2008). However, the current irrigation distribution data cannot meet the demand associated with applying a crop model at a regional scale, especially the irrigation times and amounts needed by a crop model. In order to reduce the uncertainty in regional irrigation data, those data were estimated for winter wheat production on the Loess Plateau. First of all, the irrigated and rainfed wheat areas on the Loess Plateau were classified using the method of Jin et al. (2016b). The effect of water

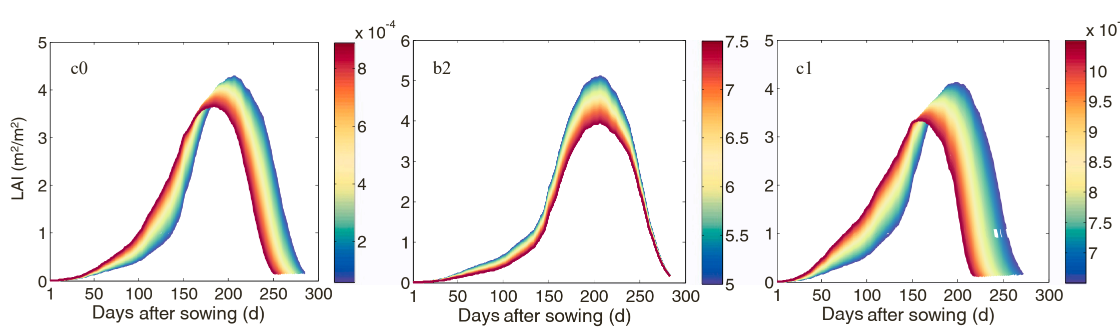

Fig. 7. Variation of leaf area index (LAI) with changes in parameters c0, b2, and c1 in the ChinaAgrosys crop model.

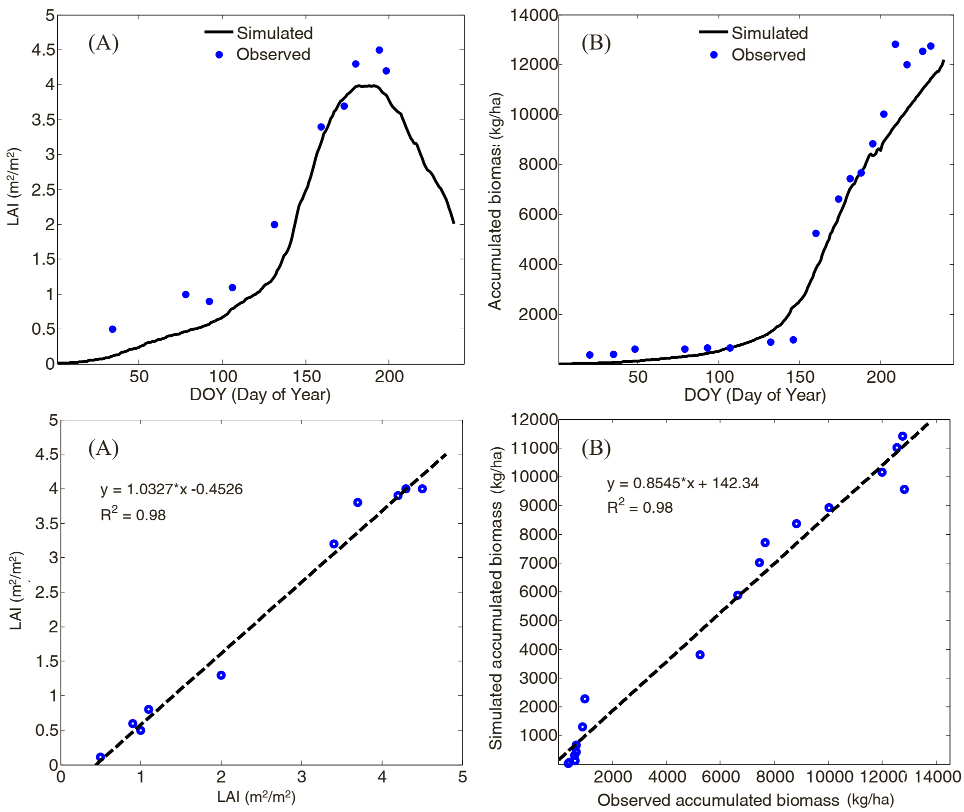

Fig. 8. Comparison of ChinaAgrosys-simulated LAI (A) and accumulated biomass (B) against observations at the Yangling, China, experimental station during 2012–2013.

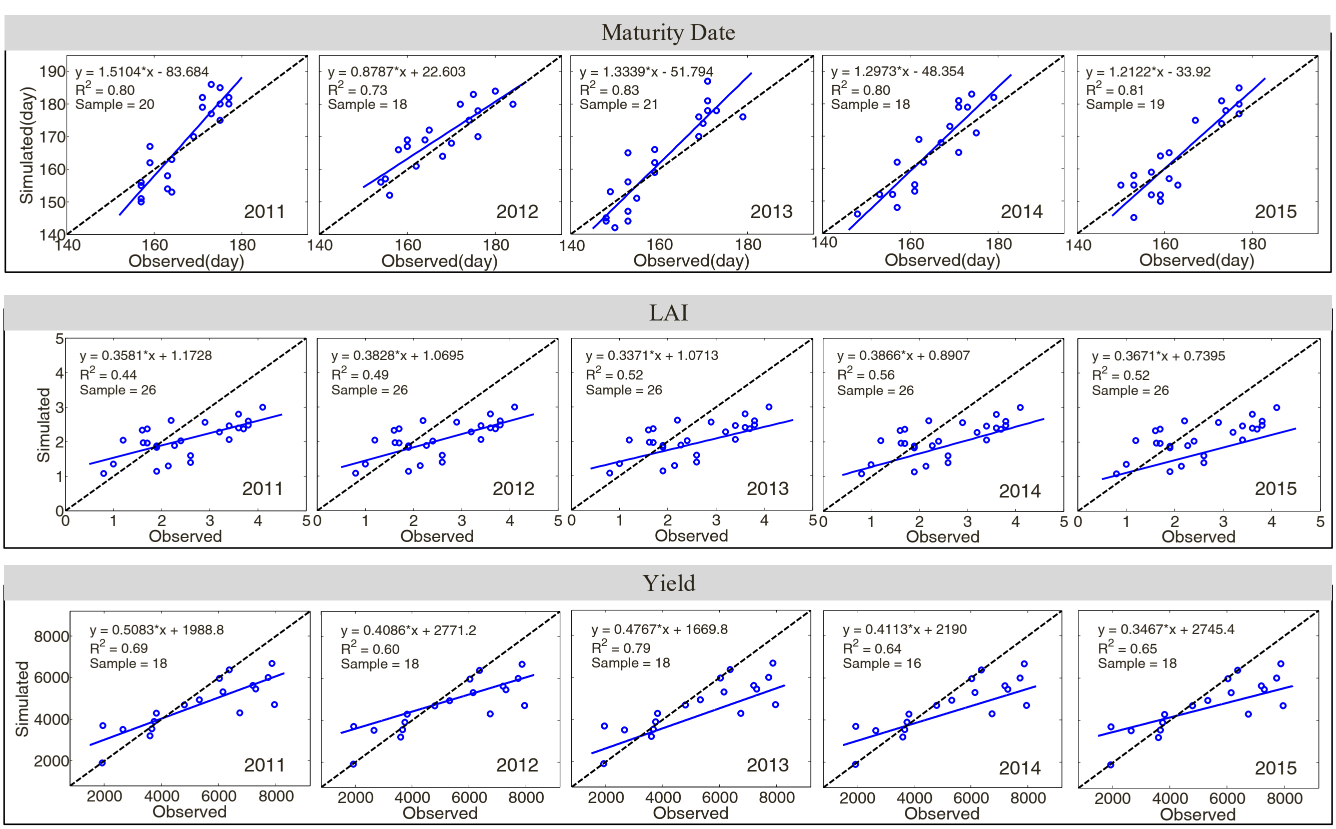

Fig. 9. Comparison of ChinaAgrosys-simulated and observed maturity date, LAI, and yield production at 21 winter wheat agrometeorological stations on the Loess Plateau from 2011 to 2015.

Table 3
Ranges of parameters to be optimized in the PROSAIL radiation transfer model.

Parameter	Interpretation	Unit	Upper limit	Lower limit
Cab	Chlorophyll a + b content	μg/cm^2	20	60
hspot	Hotspot parameter	–	0	0.8
LIDFa	Average leaf angle	degree	20	50
tto	Observer zenith angle	degree	0	10
tts	Solar zenith angle	degree	30	80

availability on winter wheat growth and phenology were taken into account by this method, and a machine learning algorithm was involved to avoid the problem of setting thresholds through repeated attempts. Secondly, winter wheat yield was estimated using a light use efficiency model, and then the irrigation times for winter wheat were deduced from the estimated yield and typical irrigation practices used on the Loess Plateau. By doing this, the uncertainty in the regional irrigation data was reduced to improve the reliability of the simulation results when assimilating remote sensing data into the crop model.

4.2. Irrigation data needs to be upscaled when applying a crop model at a regional scale

Data for driving a crop model involves meteorology, soil properties, crop management parameters, etc. Hence, upscaling this input data is the first problem to be solved when applying a crop model at a regional scale. Obtaining regional management data (especially irrigation data) is generally more difficult that upscaling meteorological and soil data. Because crop yields are largely constrained by water availability in arid and semi-arid regions, we were able to estimate irrigation times for winter wheat from wheat yield data in order to reduce the uncertainty in regional irrigation data. This irrigation estimation method goes a step further than previous studies in which crop production was treated as either rainfed or irrigated under a set, uniform irrigation scenario across the entire study area. However, the problem of upscaling irrigation data has not been completely solved since crop models need both irrigation times and amounts (Tavakoli et al., 2015).

Soil moisture increases rapidly after a crop is irrigated (Molero et al., 2016). Soil moisture at high spatial resolution is generated by downscaling the coarse-scale satellite soil moisture product (Djamai et al., 2016). Then the regional irrigation data can be estimated according to the variation of soil moisture. This method will further reduce the uncertainty in regional irrigation data and accordingly improve the simulation results of crop models assimilated with remote sensing data.

4.3. The selection of state variables and assimilation algorithm

When applying ChinaAgrosys with assimilated remote sensing data at the regional scale, the accuracy of the simulation result is mainly dependent on the accuracy of the parameters derived from remote sensing data. It is difficult to obtain a satisfactory LAI time series due to the influence of various factors such as weather conditions, observation method, spatiotemporal resolution of remote sensing data, etc. (Huang et al., 2015a). In this study, LAI was obtained using a look-up table

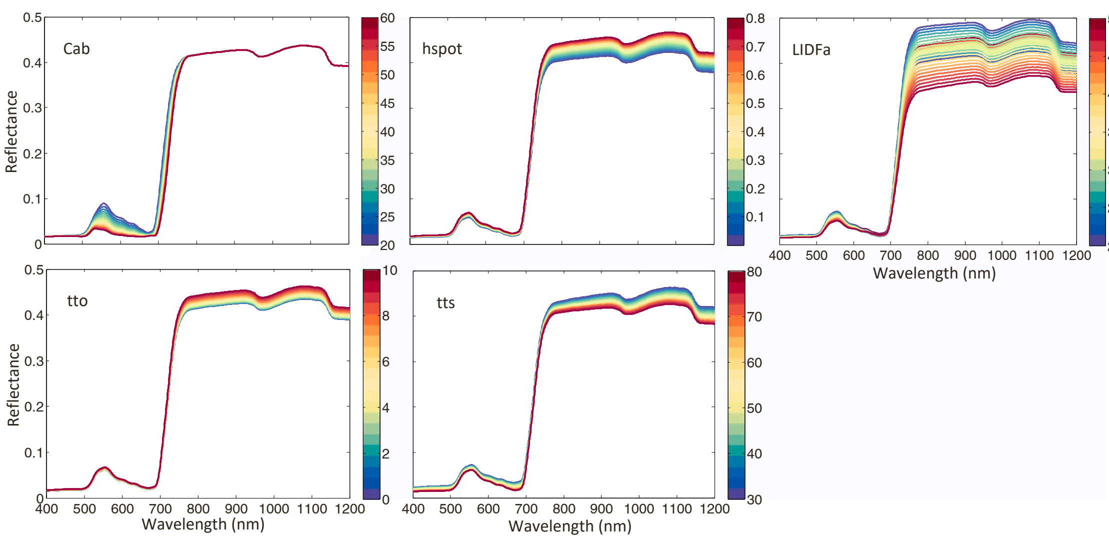

Fig. 10. Reflectance sensitivity responses for five optimization parameters in the PROSAIL radiation transfer model.

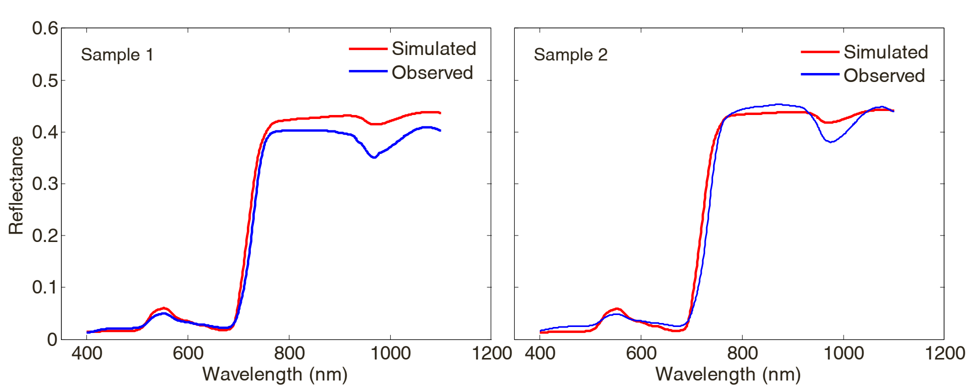

Fig. 11. Winter wheat canopy reflectance simulated by the PROSAIL radiation transfer model and ASD observations.

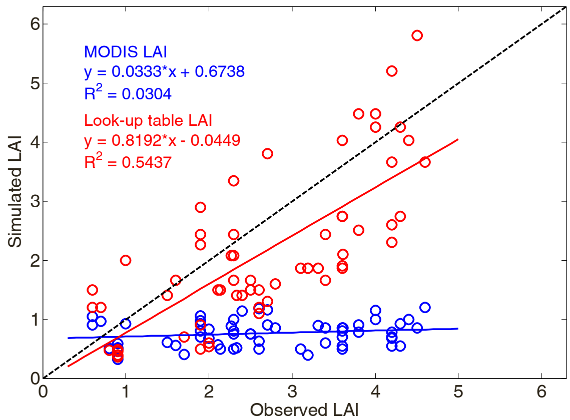

Fig. 12. Comparison of ground-observed LAI, look-up table LAI, and MODIS LAI for winter wheat.

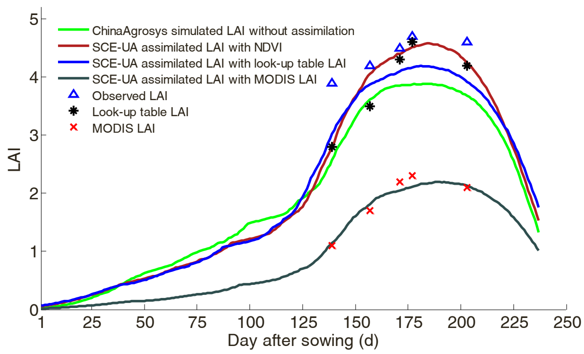

Fig. 13. Comparison of ChinaAgrosys simulated LAI and observed LAI (taking the SCE-UA algorithm as an example).

method that used inverted radiation transfer data, and the corresponding assimilation result was improved as R^2 was slightly lower but RMSE was greatly reduced compared with the assimilation result based on MODIS LAI. The assimilation result will be improved by increasing the accuracy of the inverted LAI. The assimilation result is dependent on the accuracy of the inverted parameters for the regional farmland ecosystem. Single state variables of either NDVI or LAI were used in the assimilation of remote sensing data into a crop model in this study, but two variables or multiple variables (NDVI, LAI, evapotranspiration, soil moisture, etc.) could be used together to combine the advantages of multi-source observations (Ines et al., 2013; Ma et al., 2013; Mishra et al., 2015).

Another important issue that needs to be addressed when considering the assimilation of remote sensing data into crop models is improving computational efficiency (Jin et al., 2018b). Computational efficiency is affected by various factors such as the amount of spatio-temporal data, the size of the study area, the state variables, and the algorithm used for the assimilation. The continuous assimilation algorithms of PSO and SCE-UA used in this study were time-consuming. It took at least 42.02 s to implement an assimilation process on a single pixel using an ordinary computer. The spatial resolution of the winter wheat pixel was 250 m and there were 1884 × 3815 pixels on the Loess Plateau. Consequently, it would take a relatively long time to apply a crop model assimilated with remote sensing data to all pixels due to the large amount of data. Therefore, in this study Hongtong county was selected as a representative case study to implement the assimilation of remote sensing data into a crop model.

The simulation results of crop models assimilated with remote sensing data using the PSO and SCE-UA algorithms are largely dependent on the reliability of the observed data (Liu et al., 2015). The assimilation result is improved by optimizing the parameters of the crop model, which may lack consideration of the uncertainties in both observation data and crop model simulation results. This may induce some bias in the simulation results and also may be time-consuming. Errors in the observation data and in the crop model are considered by a sequential data assimilation algorithm such as the ensemble Kalman filter (EnKF), which we plan to use in a future study. The EnKF algorithm can continuously assimilate the observed data and avoid the large number of calculations that the continuous data assimilation algorithms needed (Huang et al., 2016, 2019). The calculation efficiency for the crop model assimilated with remote sensing data can be greatly improved with the help of parallel computations and a high-performance computer (Zhao et al., 2015). Doing so will make full use of the advantages of rapidly obtaining large-scale regional data by satellite remote sensing and of the simulation products of crop models.

5. Conclusion

In this study, the spatial heterogeneity of regional irrigation data for winter wheat was considered for the Loess Plateau. Four assimilation

Table 4
Simulated winter wheat yield, simulation accuracy, and simulation computation time for ChinaAgrosys with four assimilation schemes of remote sensing data and without assimilation at the Yangling, China, experimental station in 2013–2014.

	Assimilation scheme				ChinaAgrosys without assimilation	Observation
	PSO + LAI	PSO + NDVI	SCE-UA + LAI	SCE-UA + NDVI		
Yield (kg/ha)	6874	7009	6881	6896	6537	7488
Accuracy (%)	91.8	93.6	91.9	92.1	87.3	–
Time (s)	42.02	67.37	102.87	84.69	0.3	–

Table 5
Yield estimation for rainfed and irrigated winter wheat in Hongtong county, China, in 2011.

	PSO + LAI	PSO + NDVI	SCE-UA + LAI	SCE-UA + NDVI	Light use efficiency model	ChinaAgrosys without assimilation	Statistical yield
Rainfed wheat yield (kg/ha)	2957	3548	2970	3540	3927	2430	–
Irrigated wheat yield (kg/ha)	7133	6967	6929	6192	6127	6629	–
Yield production	4113	4282	4199	4245	4301	3931	4614
Accuracy (%)	89.1	92.8	91.0	92.0	93.2	85.2	–
Average Moran's I	0.22	0.22	0.23	0.22	0.36	0.45	–

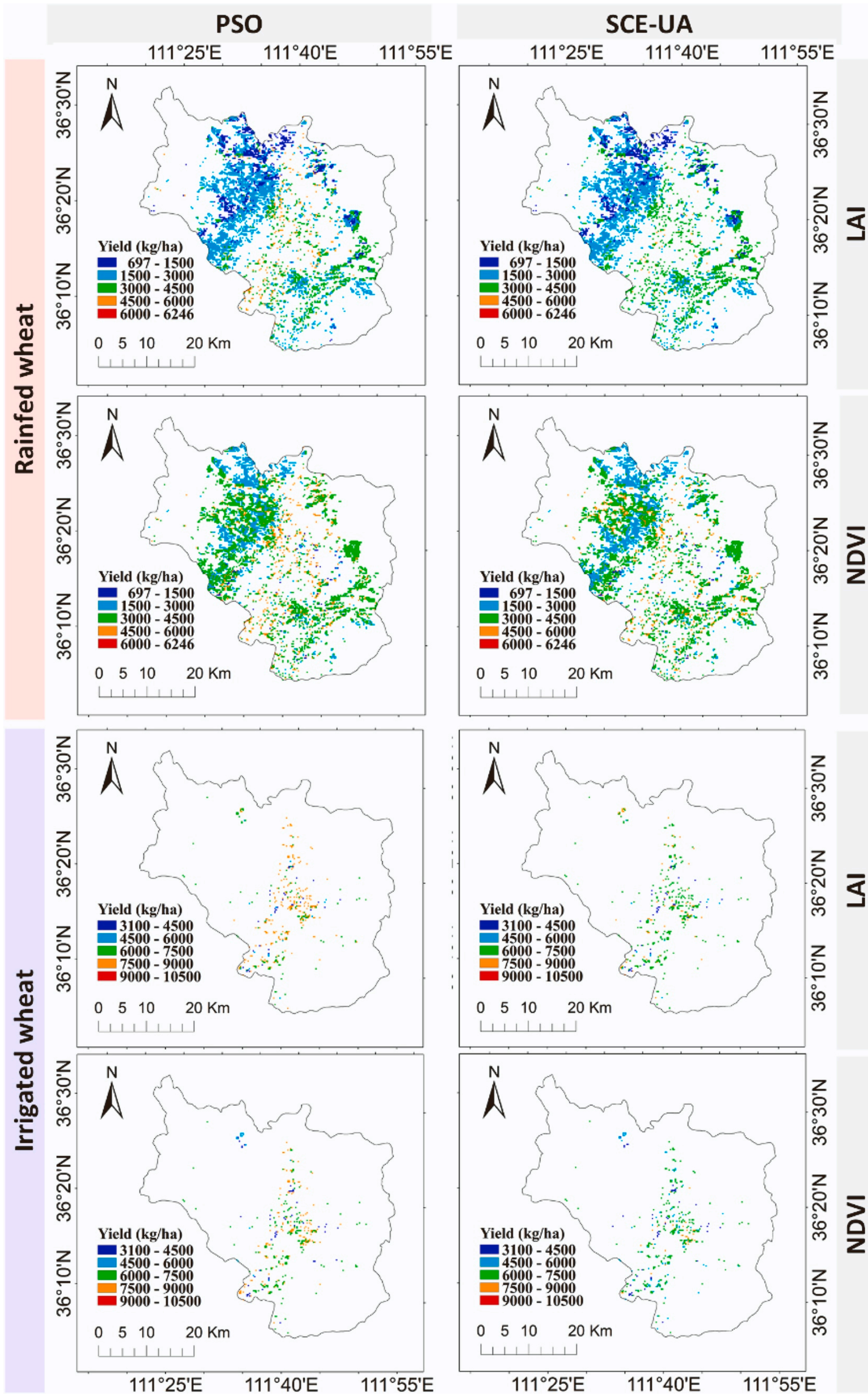

Fig. 14. Yield estimation for rainfed and irrigated winter wheat in Hongtong county, China, in 2011 when assimilating remote sensing data into the ChinaAgrosys crop model.

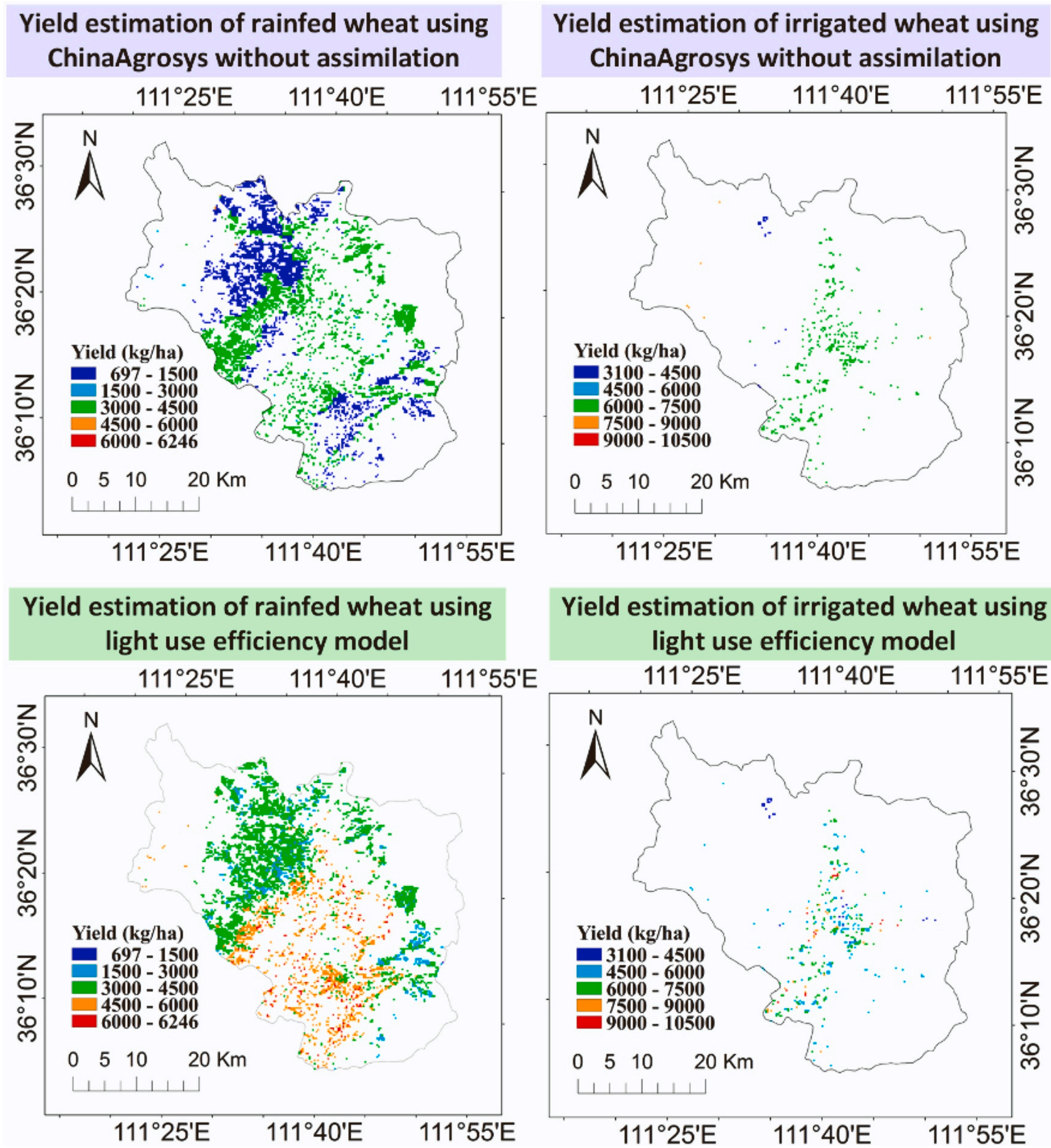

Fig. 15. Yield estimation for rainfed and irrigated winter wheat in Hongtong county, China, in 2011 using a light use efficiency model and the ChinaAgrosys crop model without assimilation of remote sensing data.

schemes were established for assimilating remote sensing data into the ChinaAgrosys crop model. The assimilation schemes were based on two state variables (LAI and NDVI) and two algorithms (PSO and SCE-UA). The productivity of winter wheat under different water availability conditions was evaluated by ChinaAgrosys with and without assimilated remote sensing data. The main conclusions of the study were: (1) rainfed wheat and wheat that was irrigated once accounted for 60.0% and 30.6%, respectively, of the wheat area, and the remaining wheat area was irrigated two or three times; (2) a look-up table of LAI values was established using inverted data from the PROSAIL radiation transfer model, and the R^2 between the observed LAI at jointing and heading stages and the inverted LAI at 250-m spatial resolution was greater than 0.54 from 2010 to 2015; (3) the global sensitivity analysis of the parameters of the ChinaAgrosys crop model showed that yield and LAI were mainly influenced by the parameters of c0, c1, and b2. The R^2 values between the ChinaAgrosys simulation results (maturity date, LAI, and yield) and the observations at 21 agrometeorologcial stations were greater than 0.73, 0.44, and 0.60, respectively, showing good applicability of ChinaAgrosys for wheat simulation on the Loess Plateau. (4) In general, the accuracy of simulation results was higher when NDVI was used as the assimilation state variable, and the calculation efficiency was higher when the PSO algorithm was used for the assimilation at both site and regional scales. The accuracy of simulation results and spatial heterogeneity for simulated winter wheat yield were improved by assimilating remote sensing data into ChinaAgrosys based on the regional irrigation data. When applying a crop model at a regional scale, accounting for spatial heterogeneity of regional irrigation data will improve the accuracy and reliability of the simulation results that are generated by assimilating remote sensing data into the crop model. Accuracy and computational efficiency of a crop model assimilated with remote sensing data should be considered together, along with the selection of the appropriate assimilation state variables and algorithms.

Declaration of Competing Interest

The authors declare that they have no known competing financial interests or personal relationships that could have appeared to influence the work reported in this paper.

Acknowledgements

We gratefully acknowledge the support of National Key Research and Development Project of China (2019YFC1510204) and Shanxi Province Colleges and Universities Science and Technology Innovation Project (2020L0729).

Compliance with Ethical Standards

Conflict of Interest: The authors declare no potential conflicts of interest for this research.

Appendix A. Supporting information

Supplementary data associated with this article can be found in the online version at doi:10.1016/j.agwat.2022.107583.

References

Adhikari, P., Ale, S., Bordovsky, J.P., Thorp, K.R., Modala, N.R., Rajan, N., Barnes, E.M., 2016. Simulating future climate change impacts on seed cotton yield in the Texas High Plains using the CSM-CROPGRO-Cotton model. Agric. Water Manag. 164, 317–330.
Bocchiola, D., Nana, E., Soncini, A., 2013. Impact of climate change scenarios on crop yield and water footprint of maize in the Po valley of Italy. Agric. Water Manag. 116, 50–61.
Casas, A., Riaño, D., Ustin, S.L., Dennison, P., Salas, J., 2014. Estimation of water-related biochemical and biophysical vegetation properties using multitemporal airborne hyperspectral data and its comparison to MODIS spectral response. Remote Sens. Environ. 148, 28–41.
Chen, Y., Zhang, Z., Tao, F.L., 2018. Improving regional winter wheat yield estimation through assimilation of phenology and leaf area index from remote sensing data. Eur. J. Agron. 101, 163–173.
Chimonyo, V.G.P., Modi, A.T., Mabhaudhi, T., 2016. Simulating yield and water use of a sorghum–cowpea intercrop using APSIM. Agric. Water Manag. 177, 317–328.
Curnel, Y., de Wit, A.J.W., Duveiller, G., Defourny, P., 2011. Potential performances of remotely sensed LAI assimilation in WOFOST model based on an OSS Experiment. Agric. Meteorol. 151, 1843–1855.
Dai, Y.J., Shangguan, W., Duan, Q.Y., Liu, B.Y., Fu, S.H., Niu, G.Y., 2013. Development of a China dataset of soil hydraulic parameters using pedotransfer functions for land surface modeling. J. Hydrometeorol. 14, 869–887.
Deines, J.M., Kendall, A.D., Crowley, M.A., Rapp, J., Cardille, J.A., Hyndman, D.W., 2019. Mapping three decades of annual irrigation across the US high plains aquifer using landsat and google earth engine. Remote Sens. Environ. 233, 111400.
Djamai, N., Magagi, R., Goïta, K., Merlin, O., Kerr, Y., Roy, A., 2016. A combination of DISPATCH downscaling algorithm with CLASS land surface scheme for soil moisture estimation at fine scale during cloudy days. Remote Sens. Environ. 184, 1–14.
Duan, Q.Y., Sorooshian, S., Gupta, V.K., 1994. Optimal use of the SCE-UA global optimization method for calibrating watershed models. J. Hydrometeorol. 158, 265–284.
Duveiller, G., Frederic, B., Defourny, P., 2013. Using thermal time and pixel purity for enhancing biophysical variable time series: an interproduct comparison. IEEE Trans. Geosci. Remote Sens. 51, 2119–2127.
Gilardelli, C., Stella, T., Confalonieri, R., Ranghetti, L., Campos-Taberner, M., García-Haro, F.J., Boschetti, M., 2019. Downscaling rice yield simulation at sub-field scale using remotely sensed LAI data. Eur. J. Agron. 103, 108–116.
Guo, C.L., Tang, Y.N., Lu, J.S., Zhu, Y., Cao, W.X., Cheng, T., Zhang, L., Tian, Y.C., 2019. Predicting wheat productivity: integrating time series of vegetation indices into crop modeling via sequential assimilation. Agric. . Meteorol. 272–273, 69–80.
Hu, S., Shi, L.S., Huang, K., Zha, Y.Y., Hu, X.L., Ye, H., Yang, Q., 2019. Improvement of sugarcane crop simulation by SWAP-WOFOST model via data assimilation. Field Crop. Res. 232, 49–61.
Huang, J.X., Tian, L.Y., Liang, S.L., Ma, H.Y., Becker-Reshef, I., Huang, Y.B., Su, W., Zhang, X.D., Zhu, D.H., Wu, W.B., 2015a. Improving winter wheat yield estimation by assimilation of the leaf area index from Landsat TM and MODIS data into the WOFOST model. Agric. Meteorol. 204, 106–121.
Huang, J.X., Ma, H.Y., Su, W., Zhang, X.D., Huang, Y.B., Fan, J.L., Wu, W.B., 2015b. Jointly assimilating MODIS LAI and ET products into the SWAP model for winter wheat yield estimation. IEEE J. Sel. Top. Appl. Earth Obs. Remote Sens. 8, 4060–4071.
Huang, J.X., Sedano, F., Huang, Y.B., Ma, H.Y., Li, X.L., Liang, S.L., Tian, L.Y., Zhang, X. D., Fan, J.L., Wu, W.B., 2016. Assimilating a synthetic Kalman filter leaf area index series into the WOFOST model to improve regional winter wheat yield estimation. Agric. Meteorol. 216, 188–202.
Huang, J.X., Gómez-Dans, J.L., Huang, H., Ma, H.Y., Wu, Q.L., Lewis, P.E., Liang, S.L., Chen, Z.X., Xue, J.H., Wu, Y.T., Zhao, F., Wang, J., Xie, X.H., 2019. Assimilation of remote sensing into crop growth models: Current status and perspectives. Agric. Meteorol. 276–277, 107609.
Ines, A.V.M., Das, N.N., Hansen, J.W., Njoku, E.G., 2013. Assimilation of remotely sensed soil moisture and vegetation with a crop simulation model for maize yield prediction. Remote Sens. Environ. 138, 149–164.
Jacquemoud, S., Verhoef, W., Baret, F., Bacour, C., Zarco-Tejada, P.J., Asner, G.P., François, C., Ustin, S.L., 2009. PROSPECT + SAIL models: a review of use for vegetation characterization. Remote Sens. Environ. 113, S56–S66.
Jin, H.A., Li, A.N., Wang, J.D., Bo, Y.C., 2016a. Improvement of spatially and temporally continuous crop leaf area index by integration of CERES-Maize model and MODIS data. Eur. J. Agron. 78, 1–12.
Jin, N., Tao, B., Ren, W., Feng, M.C., Sun, R., He, L., Zhuang, W., Yu, Q., 2016b. Mapping irrigated and rainfed wheat areas using multi-temporal satellite data. Remote Sens. 8, 207.
Jin, N., Ren, W., Tao, B., He, L., Ren, Q.F., Li, S.Q., Yu, Q., 2018a. Effects of water stress on water use efficiency of irrigated and rainfed wheat in the Loess Plateau, China. Sci. Total Environ. 642, 1–11.
Jin, X.L., Kumar, L., Li, Z.H., Feng, H.K., Xu, X.G., Yang, G.J., Wang, J.H., 2018b. A review of data assimilation of remote sensing and crop models. Eur. J. Agron. 92, 141–152.
Kang, Y.H., Özdoğan, M., 2019. Field-level crop yield mapping with Landsat using a hierarchical data assimilation approach. Remote Sens. Environ. 228, 144–163.
Kennedy, J., Eberhart, R., 1995. Particle swarm optimization Proceedings of IEEE International Conference On Neural Networks, IEEE, Perth, pp. 1942–1948.
Lei, F.N., Crow, W.T., Kustas, W.P., Dong, J.Z., Yang, Y., Knipper, K.R., Anderson, M.C., Gao, F., Notarnicola, C., Greifeneder, F., McKee, L.M., Alfieri, J.G., Hain, C., Dokoozlian, N., 2020. Data assimilation of high-resolution thermal and radar remote sensing retrievals for soil moisture monitoring in a drip-irrigated vineyard. Remote Sens. Environ. 239, 111622.
Li, Z.H., Wang, J.H., Xu, X.G., Zhao, C.J., Jin, X.L., Yang, G.J., Feng, H.K., 2015. Assimilation of two variables derived from hyperspectral data into the DSSAT-CERES model for grain yield and quality estimation. Remote Sens. 7, 12400–12418.
Liu, F., Liu, X.N., Ding, C., Wu, L., 2015. The dynamic simulation of rice growth parameters under cadmium stress with the assimilation of multi-period spectral indices and crop model. Field Crop. Res. 183, 225–234.
Loveland, T.R., Reed, B.C., Brown, J.F., Ohlen, D.O., Zhu, Z., Yang, L., Merchant, J.W., 2000. Development of a global land cover characteristics database and IGBP DISCover from 1 km AVHRR data. Int. J. Remote Sens. 21, 1303–1330.
Lv, Z.F., Liu, X.J., Tang, L., Liu, L.L., Cao, W.X., Zhu, Y., 2016. Estimation of ecotype-specific cultivar parameters in a wheat phenology model and uncertainty analysis. Agric. Meteorol. 221, 219–229.
Mishra, A.K., Ines, A.V.M., Das, N.N., Khedun, C.P., Singh, V.P., Sivakumar, B., Hansen, J.W., 2015. Anatomy of a local-scale drought: Application of assimilated remote sensing products, crop model, and statistical methods to an agricultural drought study. J. Hydrometeorol. 526, 15–29.
Mo, X., Liu, S., Lin, Z., Xu, Y., Xiang, Y., McVicar, T.R., 2005. Prediction of crop yield, water consumption and water use efficiency with a SVAT-crop growth model using remotely sensed data on the North China Plain. Ecol. Model. 183, 301–322.
Molero, B., Merlin, O., Malbéteau, Y., Bitar, A.A., Cabot, F., Stefan, V., Kerr, Y., Bacon, S., Cosh, M.H., Bindlish, R., Jackson, T.J., 2016. SMOS disaggregated soil moisture product at 1 km resolution: Processor overview and first validation results. Remote Sens. Environ. 180, 361–376.
Moran, P.A.P., 1950. Notes on continuous stochastic phenomena. Biometrika 37, 17–23.
Ozdogan, M., Gutman, G., 2008. A new methodology to map irrigated areas using multi-temporal MODIS and ancillary data: An application example in the continental US. Remote Sens. Environ. 112, 3520–3537.
Park, S., Im, J., Jang, E., Rhee, J., 2016. Drought assessment and monitoring through blending of multi-sensor indices using machine learning approaches for different climate regions. Agric. Meteorol. 216, 157–169.
Pasolli, L., Asam, S., Castelli, M., Bruzzone, L., Wohlfahrt, G., Zebisch, M., Notarnicola, C., 2015. Retrieval of leaf area index in mountain grasslands in the alps from modis satellite imagery. Remote Sens. Environ. 165, 159–174.
Pervez, M.S., Budde, M., Rowland, J., 2014. Mapping irrigated areas in Afghanistan over the past decade using MODIS NDVI. Remote Sens. Environ. 149, 155–165.
Sakamoto, T., Gitelson, A.A., Arkebauer, T.J., 2013. MODIS-based corn grain yield estimation model incorporating crop phenology information. Remote Sens. Environ. 131, 215–231.
Steven, M.D., Malthus, T.J., Baret, F., Xu, H., Chopping, M.J., 2003. Intercalibration of vegetation indices from different sensor systems. Remote Sens. Environ. 88, 412–422.
Tavakoli, A.R., Moghadam, M.M., Sepaskhah, A.R., 2015. Evaluation of the AquaCrop model for barley production under deficit irrigation and rainfed condition in Iran. Agric. Water Manag. 161, 136–146.
Wang, J., Yu, Q., Lee, X.H., 2007. Simulation of energy and CO_2 fluxes and crop growth at different time steps from hourly to daily. Hydrol. Process. 21, 2474–2492.
Wang, X.P., Huang, G.H., Yang, J.S., Huang, Q.Z., Liu, H.J., Yu, L.P., 2015. An assessment of irrigation practices: Sprinkler irrigation of winter wheat in the North China Plain. Agric. Water Manag. 159, 197–208.
de Wit, A.J.W., van Diepen, C.A., 2007. Crop model data assimilation with the Ensemble Kalman filter for improving regional crop yield forecasts. Agric. Meteorol. 146, 38–56.
Xie, Y.H., Lark, T.J., Brown, J.F., Gibbs, H.K., 2019. Mapping irrigated cropland extent across the conterminous United States at 30 m resolution using a semi-automatic training approach on Google Earth Engine. ISPRS J. Photogramm. Remote Sens. 155, 136–149.

Yin, Y.Y., Zhang, X.M., Lin, D.G., Yu, H., W, J.A., Shi, P.J., 2014. GEPIC-V-R model: a GIS-based tool for regional crop drought risk assessment. Agric. Water Manag. 144, 107–119.

Zhang, T.Y., Simelton, E., Huang, Y., Shi, Y., 2013. A Bayesian assessment of the current irrigation water supplies capacity under projected droughts for the 2030s in China. Agric. Meteorol. 178–179, 56–65.

Zhao, G., Siebert, S., Enders, A., Rezaei, E.E., Yan, C.Q., Ewert, F., 2015. Demand for multi-scale weather data for regional crop modeling. Agric. Meteorol. 200, 156–171.